Received: 8 August 2021 | Revised: 19 September 2021 | Accepted: 1 October 2021

DOI: 10.1002/cey2.172

RESEARCH ARTICLE

CARBON ENERGY WILEY

TiO_2 bunchy hierarchical structure with effective enhancement in sodium storage behaviors

Shen Liu | Kai Niu | Shuailin Chen | Xin Sun | Lehao Liu | Bing Jiang | Lihua Chu | Xiaojun Lv | Meicheng Li

State Key Laboratory of Alternate Electrical Power System with Renewable Energy Sources, North China ElectricPower University, Beijing, China

Correspondence
Meicheng Li, State Key Laboratory of Alternate Electrical Power System with Renewable Energy Sources, North China ElectricPower University, 102206 Beijing, China.
Email: mcli@ncepu.edu.cn

Abstract

Bronze phase TiO_2 [TiO_2(B)] has great research potential for sodium storage since it has a higher theoretical capacity and ion mobility compared with other phases of TiO_2. In this case, preparing porous TiO_2(B) nanosheets, which can provide abundant sodium insertion channels, is the most effective way to improve transport kinetics. Here, we use the strong one-dimensional TiO_2 nanowires as the matrix for stringing these nanosheets together through a simple solvothermal method to build a bunchy hierarchical structure [TiO_2(B)-BH], which has fast pseudocapacitance behavior, high structural stability, and effective ion/electron transport. With the superiorities of this structure design, TiO_2(B)-BH has a higher capacity (131 vs. 70 mAh g^{-1} [TiO_2-NWs] at 0.5 C). And it is worth mentioning that the reversible capacity of up to 500 cycles can still be maintained at 85 mAh g^{-1} at a high rate of 10 C. Meanwhile, we also further analyzed the sodium storage mechanism through the ex-situ X-ray powder diffraction test, which proved the high structural stability of TiO_2(B)-BH in the process of sodiumization/de-sodiumization. This strategy of uniformly integrating nanosheets into a matrix can also be extended to preparing electrode material structures of other energy devices.

KEYWORDS

hierarchical, porous, sodium-ion batteries, TiO_2 bronze phase nanosheets

1 | INTRODUCTION

In the 1980s, lithium-ion batteries (LIBs) and sodium-ion batteries (SIBs) were proposed simultaneously.[1,2] So far, LIB is still regarded as the most potential energy storage battery. Stimulated by Sony's successful commercialization in the 1990s, its application density in energy storage power stations and electric vehicles (EV) has increased. However, compared with the lithium content, sodium resources are more abundant and extensive.[3] In addition, when considering electrochemical principles similar to LIB, SIB may be more privileged than other energy storage batteries.[4,5] Not surprisingly, SIB has grown rapidly in recent decades.

However, due to concerns about the high ionization potential and radius of sodium ions, there is a great need to develop suitable electrode materials for sodium-ion batteries. For the anode material, it is divided into three

types according to its charge and discharge mechanism. Alloying/dealloying materials, such as Sn,[6,7] Sb,[8–10] and P,[11–13] generally have serious volume changes in the process of sodiumization and de-sodiumization, which can easily lead to follow-up pulverization, endangering battery safety. The initial Coulombic efficiency of the conversion reaction electrode will be very low, and there will be a higher potential hysteresis.[14,15] The electrode material of the insertion/extraction reaction type is still the researcher's favorite. As a classic candidate for insertion, titanium-based anode materials have attracted great attention from the scientific community.[16–18]

For titanium dioxide (TiO_2), it is one of the most potential SIB candidate materials due to its rich content, nonpolluting nature, stability, and safety.[19] Thanks to its own pseudo-capacitance behavior, TiO_2 has nice sodium storage performance.[20–22] However, TiO_2 is a semiconductor that cannot be used well in the negative electrode of sodium ion batteries.[23] Among the polymorphs of titanium dioxide, TiO_2(B) can provide more insertion sites and diffusion paths by its open-channel framework. The fast pseudo-capacitance sodiumization/desodiumization behavior leads to an increase in the maximum theoretical capacity to 335 mAh g^{-1}.[24,25] The calculation results by Dawson and Robertson showed that TiO_2(B) is more suitable for Na^+ ion intercalation than anatase and rutile TiO_2.[26] Legrain et al. showed that TiO_2(B) can reduce the formation energy of Na^+ insertion defects compared with anatase and rutile TiO_2, which is consistent with the former research.[27] However, the inherent shortcomings still reduce the potential of TiO_2(B) as an anode material for SIBs.[28,29] In addition, TiO_2(B) is not stable, and it is easy to generate a stable phase through irreversible phase transition during the sodiumization/desodiumization process,[30] resulting in poor cycle stability. Moreover, due to low thermodynamic stability, TiO_2(B) nanosheets will agglomerate into a powder state during deep cycles, which will reduce the conductivity and cycle stability of the electrode. Therefore, improving the long-term cycling stability of TiO_2(B) nanosheets is important for their application in SIBs.

In this article, we use a self-assembly strategy to integrate TiO_2(B) nanosheets on a one-dimensional (1D) nanowire matrix to build a TiO_2 bunchy hierarchical structure. This structure prevents the nanosheets from crushing, agglomerating, or peeling off during repeated sodiumization/de-sodiumization processes, thereby improving the structural stability of the entire hierarchical system. A vast number of micro-TiO_2(B) nanosheets provide a wide electrode/electrolyte interface contact area, which promotes rapid charge transfer and psedocapacitance manners. This synthesis strategy effectively improves the capacity (131 mAh g^{-1}) and rate performance (92 mAh g^{-1} at 3350 mA g^{-1}) of the TiO_2 anode material in SIB, showing a huge practical application potential.

2 | RESULTS AND DISCUSSION

Here, a simple hydrothermal method of 1D TiO_2 nanowires prepared with Ag cations as a medium was used to build this structure. The schematic process was shown in Scheme 1. The TiO_2 nanowires prepared were used as the basis, which is essential for constructing the structure. If TiO_2 nanowires are not added, TiO_2(B) nanosheets will self-stack into spheres by adding Ag^+ (Figure S1B). In the above process, different amounts of Ag^+ will also cause the morphology of the product to be different (Figure S2). This difference may have an impact on the performance of the battery.

As shown in the scanning electron microscope (SEM) image (Figure 1A,B), the elongated structure of one-dimensional TiO_2 nanowires supports the growth of densely packed ultra-thin nanosheets. The mechanism of sodium ion deintercalation and transport caused by its surface morphology is shown in Figure 1C. Many porous nanosheets grow around the belt to form a 3D hierarchical structure. On the basis of using the intercalation and deintercalation mechanism to store sodium ions, the structure also provides a channel for sodium ions, which improves the sodium storage performance of the battery. Transmission electron microscopy (TEM) images further

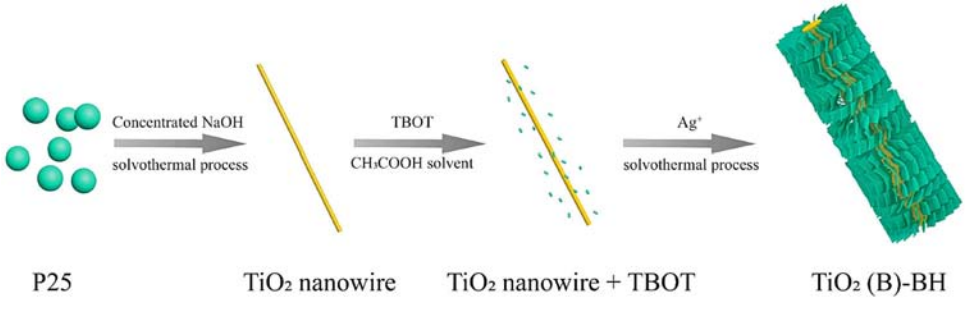

SCHEME 1 Illustration of the preparation of the TiO_2(B)-BH

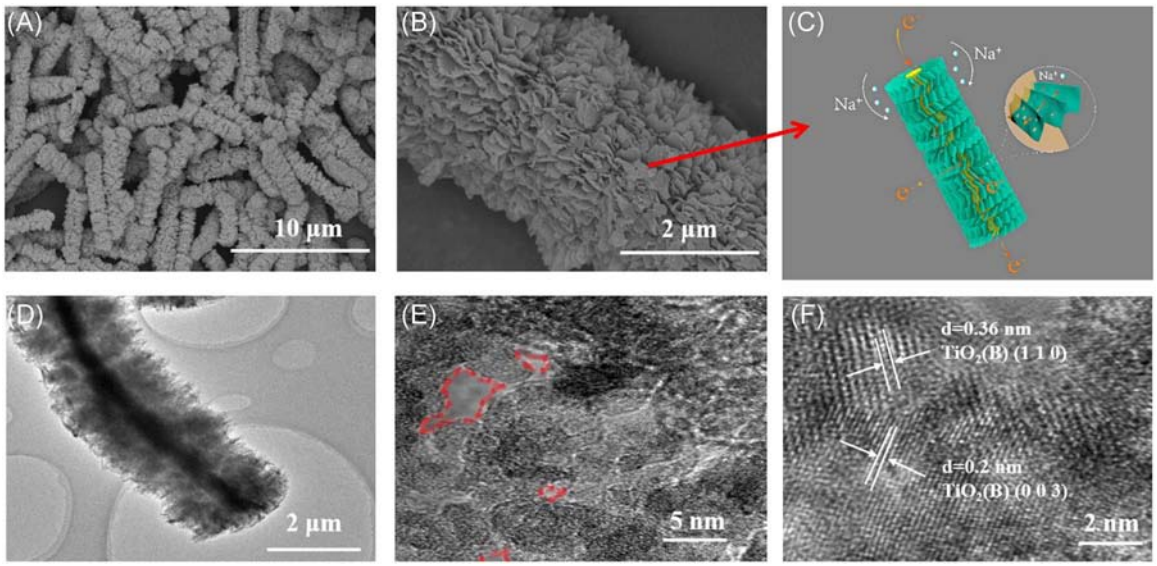

FIGURE 1 (A,B) SEM image of TiO_2(B)-BH (C) TiO_2(B)-BH sodium ion transmission path diagram (D) TEM image of TiO_2(B)-BH (E,F) HRTEM images of TiO_2 nanosheets over the surface of TiO_2(B)-BH. HRTEM, high-resolution transmission electron microscopy; SEM, scanning electron microscope; TEM, transmission electron microscopy

clarify the TiO_2(B)-BH in detail, and it can be seen that a 1D nucleus exists in the center (Figure 1D). The size of the center is the same as that of the added TiO_2 nanowires; we can say TiO_2 nanowires effectively string the porous nanosheets together. The important thing is that the thickness of the integrated TiO_2 nanosheets (>1 μm) on the 1D TiO_2 nanowires, which is much larger than the thickness of the thin TiO_2 layer (<100 nm) in the previous report.[31,32] Taking into account the 0–2.5 V safe operating window, thicker layers can increase the loading rate and the usage rate of the active material (TiO_2) in the electrode. The high-resolution transmission electron microscopy (HRTEM) image (Figure 1E) shows that the TiO_2(B) nanosheets have about 5 nm nanopores (marked with red lines). In Figure 1E, the lattice fringes of the nanosheets can be clearly observed, indicating that the crystal structure is clear. EDS shows that oxygen and titanium are uniformly distributed in TiO_2(B)-BH (Figure S3). It can be seen in Figure S4 that there is still a small amount of Ag^+ on TiO_2(B)-BH, and Ag^+ promotes the conduction of electrons, expands the layer spacing of TiO_2(B) nanosheets, and provides more sodium storage space for the material.[33]

In addition, X-ray powder diffraction (XRD) analysis was performed on the structure of the material, as shown in Figure 2A. The synthesized TiO_2(B)-BH has a monoclinic B-phase structure and the space group is C2/m. In the test results, the highest diffraction peak appears at 25°, which corresponds to the (110) plane. The result is completely consistent with the PDF card of TiO_2(B) (JCPDS 046-1238), which is in good agreement with the HRTEM observation. All the results show that we have obtained the TiO_2(B)-BH by stringing a large number of TiO_2(B) nanosheets on the nanowires. The adsorption isotherm is shown in Figure 2B. The curve shows the presence of nanopores in the material, which is formed mainly by the stacking of nanosheets.[34] According to the Barrett-Joyner-Halenda pore size distribution diagram, the pore size on the nanosheet is about 5–7 nm, which corresponds to the TEM observation. TiO_2(B)-BH has a high specific surface area (198 $m^2 g^{-1}$)and pore volume (0.80 $cm^3 g^{-1}$). Moreover, the gap between nanosheets is larger, which can be verified by the differentiated pore distributions and TEM images. As we all know, a larger specific surface area provides a wider electrode/electrolyte interface which can reduce interface resistance and accelerate sodium ion diffusion, thereby improving the rate performance of SIBs. In this case, TiO_2(B)-BH has shown broad prospects at a high rate as SIB anode material.

We assembled TiO_2(B)-BH into Na half-cells and conducted a series of electrochemical tests. Figure 3A shows the cyclic voltammetry curve of the battery between 0 and 2.5 V during the first three cycles. The position of the reduction peak in the first circle is approximately 0.5 V because of the formation of a stable solid electrolyte interphase (SEI) and the irreversible decomposition of the electrolyte.[35,36] It is also possible that Na^+ is irreversibly inserted into the structural defect crystals of TiO_2.[37] In the next two scans, the position of the reduction peak is around 0.76 V, and the position of the oxidation peak is around 0.84 V, which proves that there is a reversible reduction/oxidation process between Ti^{4+} and Ti^{3+}. Obviously, there

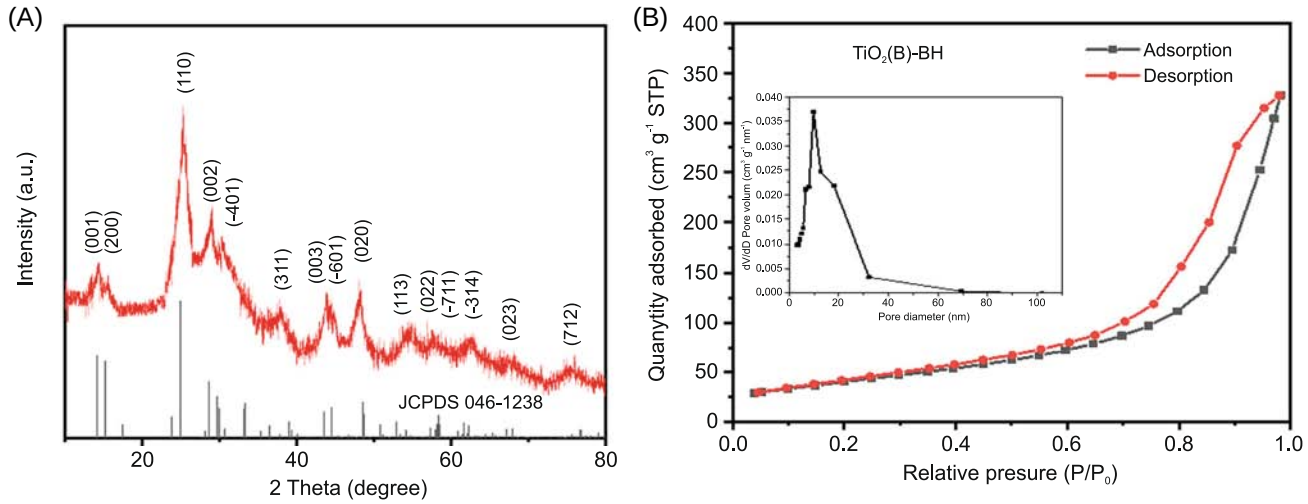

FIGURE 2 (A) XRD pattern of TiO_2(B)-BH and standard JCPDS card of TiO_2(B); (B) adsorption–desorption isotherms of TiO_2(B)-BH (inset is corresponding pore size distribution curves). XRD, X-ray powder diffraction

is a lower deviation between the redox peaks in the TiO_2(B)-BH electrode (voltage deviation between the anode peak and the cathode peak ($\Delta E = 0.08$ V)) and obvious peak intensity were observed, indicating the structural design improved the kinetics of the TiO_2(B) anode. Figure 3B shows the galvanostatic discharge–charge curve of the battery in the 0–2.5 V potential window at a current density of 0.5 C. The wide plateau during discharge and charging of 0.6–0.9 V is caused by the reversible insertion/deintercalation of Na^+. The plateau period of the first five turns of the discharge curve is the highest among all the curves, which agrees well with the cyclic voltammetry (CV) result. The initial Coulombic efficiency of the TiO_2(B)-BH electrode at 0.5 C is 41.2% because of the loss of sodium ions resulting from the formation of the SEI film. After the 50th and 100th cycles, there is no significant difference in the charge–discharge curve of the battery. It indicates that the electrode has high cycle stability during long-term operation. After 100 cycles, the TiO_2(B)-BH anode can maintain a high specific capacity of 131 mAh g^{-1} (Figure 3C). The low initial Coulombic capacity loss is mainly ascribed to the interfacial reaction between electrolyte and the active substance on/in TiO_2(B), such as inevitable oxygen, water or active impurity. Unlike lithium-ion batteries, the Coulombic efficiency is basically stable at about 100% after 10 cycles. The instability of the curve in the first 50 cycles may be due to the unevenness of the sodium foil and the activation of the porous electrode. For the TiO_2-NWs electrode, its initial capacity value is 115.5 mAh g^{-1} at 0.5 C. After 100 discharge–charge cycles, the specific capacity drops rapidly and finally remains at 70 mAh g^{-1}. The TiO_2(B)-BH also shows good rate performance from 0.2 to 10 C. As shown in Figure 3D, it can be clearly seen that the SIB of the TiO_2(B)-BH electrode has a high specific capacity at each rate, which shows that the unique advantage of the bunchy hierarchical structure. It can transmit electrons more effectively, and the ion adsorption/diffusion kinetics is improved. At the same time, we also made a comparison in electrochemical performance with TiO_2(B)-nanosphere and P25 (Figure S4). Obviously, the specific capacity of TiO_2(B)-nanosphere and P25 is also much lower than that of TiO_2(B)-BH, proving the contribution of this structure to high capacity. To further study the cycle stability of the sample as an anode material for SIBs, TiO_2(B)-BH was run for 500 cycles at a high current density of 10 C, and it still showed the capacity of 85 mAh g^{-1}. In particular, the Coulombic efficiency climbed to 98% after 30 cycles, and the specific capacity remained basically unchanged. Compared with the sodium storage capacity of bronze and anatase titanium dioxide in other works (Table S1), the TiO_2(B)-BH electrode prepared in this study has good cycle performance and longevity due to its unique structure.

To deeply study the good rate performance of the TiO_2(B)-BH anode, we studied the reaction kinetics through altering scan rate of CV tests. In Figure 4A,B, we can see that CV curves under different scan rates show similar shapes and broad peaks. Figure 4C,D shows the $\log(i)$ and $\log(v)$ graphs of the reduction peak and the oxidation peak of the TiO_2(B)-BH electrode in the scan rate range of 0.2–1.2 mV s^{-1}. The current shows a relationship related to the scan rate[38]:

$$i = av^b. \tag{1}$$

The b-value of 0.5 represents a diffusion-controlled process, whereas the b-value of 1 represents a capacitance-controlled process. For the reduction and oxidation peaks, the b values of the TiO_2(B)-BH electrode are 0.76971 and

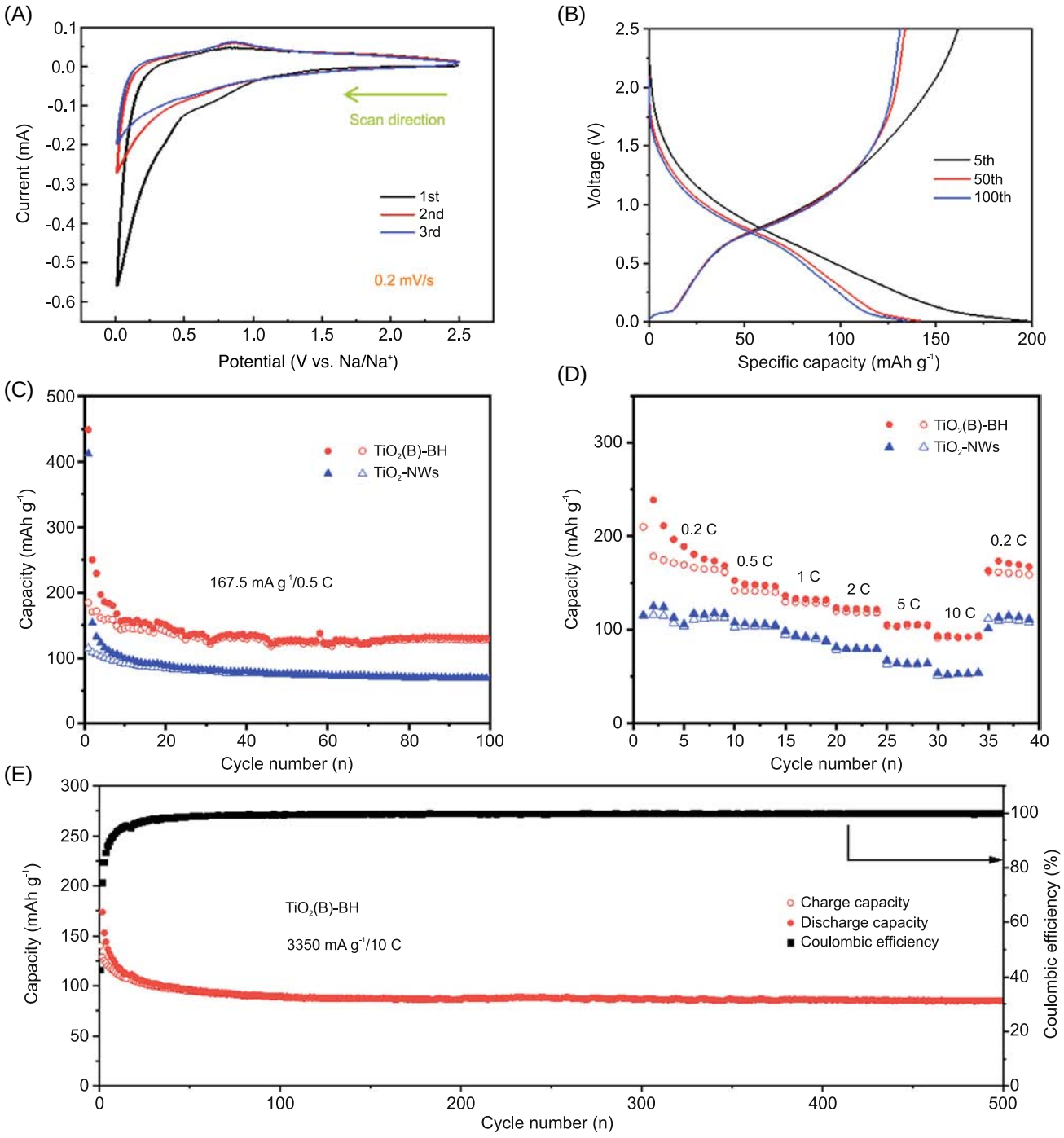

FIGURE 3 (A) CV curve of TiO_2(B)-BH at the scan rate of 0.2 mV s^{-1} for the first, second, and third cycles; (B) charge and discharge curve at 0.5 C; (C) TiO_2(B)-BH electrode cycle performance at 0.5 C (167.5 mA g^{-1}); (D) rate performance; and (E) long-term cycle performance at a rate of 10 C. CV, Cyclic Voltammetry

0.93231, respectively, which indicates that the sodium storage process is mainly a surface capacitance effect. In addition, we can also quantify the contribution rate of diffusion and capacitance by the following equation[39,40]:

$$i(V) = k_1 v + k_2 v^{1/2}. \quad (2)$$

In Equation 2, $k_1 v$ and $k_2 v^{1/2}$ correspond to the current contributions from the surface capacitive effects and the diffusion-controlled intercalation process, respectively. Thus, by determining k_1 and k_2, we are able to quantify, at specific potentials, the fraction of the current due to each of these contributions.

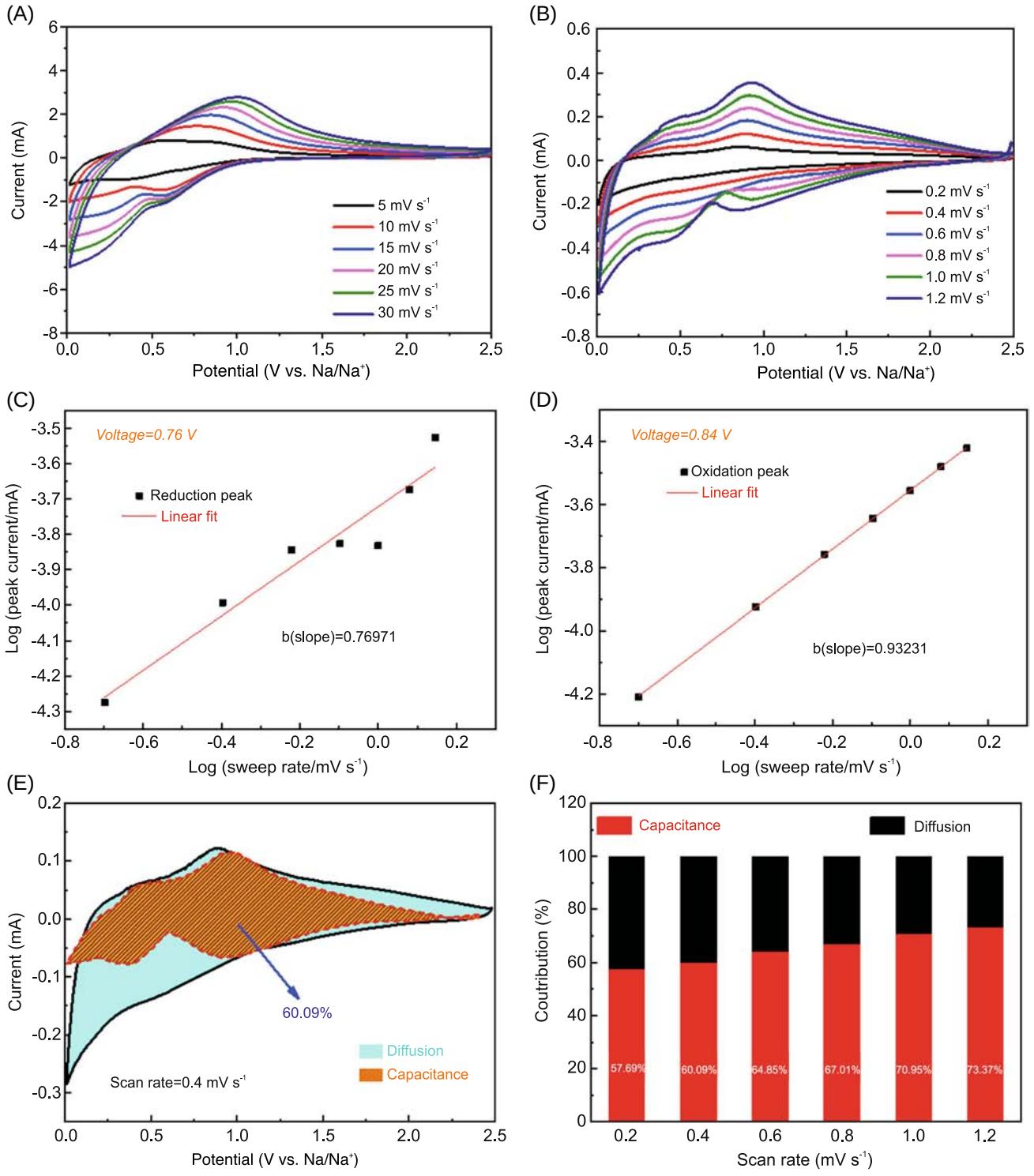

FIGURE 4 Sodium storage kinetics for the TiO_2(B)-BH electrode. (A) CV curves at different scan rates of 5–30 mV s^{-1}. (B) CV curves over the scan rate range of 0.2-1.2 mV s^{-1}. (C,D) *b*-value analysis using the relationship between the peak current and the scan rate. (E) Separation of the capacitive (shaded region) and diffusion currents in the TiO_2(B)-BH electrode at the scan rate of 0.4 mV s^{-1}. (F) Contribution ratio of the capacitive and diffusion-controlled charges at different scan rates. CV, Cyclic Voltammetry

As shown in Figures 4E, 69.0% of the total charge corresponds to the "capacitance" contribution at 0.4 mV s^{-1}. The remaining part corresponds to the charge controlled by diffusion, which almost occurs in the peak voltage. It represents the oxidation–reduction reaction between Ti^{4+}/Ti^{3+}.[41] We can also calculate the contribution of capacitance and diffusion at other scan rates by using the equations mentioned above. At a scan rate

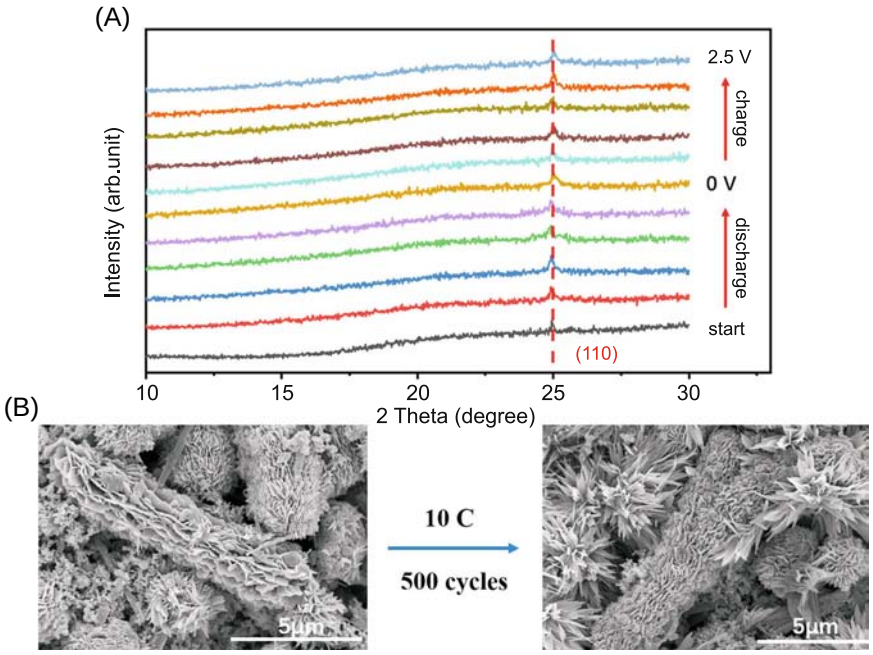

FIGURE 5 (A) Ex situ XRD patterns of TiO_2(B)-BH anode during the first cycle with a constant current of 0.2 C rate. (B) SEM image of initial TiO_2(B)-BH and that after 500 cycles. SEM, scanning electron microscope; XRD, X-ray powder diffraction

of 0.6 mV s^{-1} (Figure 4F), the capacitance contribution rate of the TiO_2(B)-BH electrode reaches 64.85%. As the scan rate increases, the contribution rate of the capacitance gradually rises. Therefore, we can infer that the high capacitance contribution rate can significantly improve the rate and cycle performance of the electrode. This pseudo-capacitance effect is caused by the high specific surface area of the TiO_2(B)-BH, that is, hole defects in the ordered nanosheets around the titanium oxide nanowires, the spacing between the nanosheets, and the interface between the nanosheets and the nanowires.

We performed an ex-situ XRD analysis on TiO_2(B)-BH to have a deeper understanding of the sodium storage mechanism. As shown in Figure 5A, the (110) characteristic peak at about 25° (2θ) shifts slightly to the left due to the expansion of the crystal lattice during the initial discharge process. It indicates the reaction is not conversion of TiO_2 to Ti metal, but is the electrochemical reduction of $Ti^{4+/3+}$.[36,42] This corresponds to the position of the oxidation peak (0.84 V) and the reduction peak (0.76 V) in the 2nd and 3rd cycles in Figure 3A,B. During the charging process, the detachment of sodium ions causes the structure to shrink, and the characteristic peaks return to their original positions. The reaction equations between sodium and TiO_2 are as follows:[41]

$$TiO_2 + xNa^+ + xe^- \leftrightarrow Na_x\left(Ti_x^{3+}Ti_{1-x}^{4+}\right)O_2. \quad (3)$$

The results show that the structure of this bunchy hierarchical structure has a very good effect on the reversible insertion of sodium ions into the main structure of the electrode material. The structure and morphology of TiO_2(B)-BH after 500 cycles are shown in Figure 5B. The volume of TiO_2(B) nanosheets is reduced and partly falls off during charging and discharging, but TiO_2(B)-BH can still maintain the bunchy hierarchical structure during the continuous sodiumization/de-sodiumization process due to the 1D nanowires as the core is not destroyed. It indicates that TiO_2(B)-BH maintains a high degree of structural stability during the sodium insertion/extraction process.

3 | CONCLUSIONS

In summary, we built TiO_2(B)-BH by stringing porous TiO_2(B) nanosheets on TiO_2 nanowires to gain high capacity and good recyclability of SIB. The core is a 1D nanowire, which occupies a very small solid volume in the bunchy hierarchical structure, resulting in a shortened electron/ion path. In addition, this structure reduces the volume expansion during charging and discharging, and thereby TiO_2(B)-BH has very high stability. TiO_2(B)-BH can achieve a high reversible capacity (131 mAh g^{-1} at 0.5 C) and good rate performance (92 mAh g^{-1} at 10 C). In addition, the reversible capacity

of sodium-ion batteries can be maintained at 85 mAh g^{-1} even after 500 cycles at 10 C. This integrated strategy of nanoscale construction can also be used in the structure design of materials for LIBs, Mg-ion batteries, lithium-sulfur batteries, supercapacitors, and so on.

ACKNOWLEDGMENTS

This study is supported partially by the Natural Science Foundation of Beijing Municipality (L172036), Joint Funds of the Equipment Pre-Research and Ministry of Education (6141A020225), Par-Eu Scholars Program, Science and Technology Beijing 100 Leading Talent Training Project, the Fundamental Research Funds for the Central Universities (2020FR002, 2020MS023, 2020MS028, 2021MS028), and the NCEPU "Double First-Class" Program, the State Key Laboratory of Alternate Electrical Power System with Renewable Energy Sources (LAPS21004).

CONFLICT OF INTEREST

The authors declare no conflict of interest.

REFERENCES

1. Parant JP, Olazcuaga R, Devalette M, Fouassier C, Hagenmuller P. Sur quelques nouvelles phases de formule Na_xMnO_2 ($x \leqslant 1$). *J Solid State Chem*. 1971;3(1):1-11.
2. Mizushima K, Jones PC, Wiseman PJ, Goodenough JB. Li_xCoO_2 ($0 < x \leq 1$): a new cathode material for batteries of high energy density. *Solid State Ionics*. 1981;3-4:171-174.
3. Pan H, Hu YS, Chen L. Room-temperature stationary sodium-ion batteries for large-scale electric energy storage. *Energy Environ Sci*. 2013;6(8):2338-2360.
4. Liu N, Wang B, Chen S, et al. Use of a novel layered titanoniobate as an anode material for long cycle life sodium ion batteries. *RSC Adv*. 2016;6(42):1-4.
5. Bommier C, Ji X. Recent development on anodes for Na-ion batteries. *Isr J Chem*. 2015;55(5):1-23.
6. Tomboc GM, Wang YT, Wang H, Li JH, Lee K. Sn-based metal oxides and sulfides anode materials for Na ion battery. *Energy Stor Mater*. 2021;39:21-44.
7. He W, Chen K, Pathak R, Hummel M, Zhou Y. High-mass-loading Sn-based anode boosted by pseudocapacitance for long-life sodium-Ion batteries. *Chem Eng J*. 2021;414:128638.
8. Sarkar S, Roy S, Zhao YF, Zhang JJ. Recent advances in semimetallic pnictogen (As, Sb, Bi) based anodes for sodium-ion batteries. *Nano Res*. 2021(11):1-34.
9. Jing WT, Yang C, Jiang Q. Recent progress on metallic Sn- and Sb-based anodes for sodium-ion batteries. *J Mater Chem A*. 2020;8(6):2913-2933.
10. Liang SZ, Cheng YJ, Zhu J, Xia YG, Muller-Buschbaum P. A chronicle review of nonsilicon (Sn, Sb, Ge)-based lithium/sodium-ion battery alloying anodes. *Small Methods*. 2020;4(8):2000218.
11. Shen LY, Shi SS, Roy S, Yin XP, Liu WB, Zhao YF. Recent advances and optimization strategies on the electrolytes for hard carbon and P-based sodium-ion batteries. *Adv Funct Mater*. 2021;31(4):2006066.
12. Hameed AS, Ohara M, Kubota K, Komaba S. A phosphite-based layered framework as a novel positive electrode material for Na-ion batteries. *J Mater Chem A*. 2021;9(8):5045-5052.
13. Yan J, Li H, Wang K, et al. Ultrahigh phosphorus doping of carbon for high-rate sodium ion batteries anode. *Adv Energy Mater*. 2021;11(21):2003911.
14. Zhang Y, Zhu P, Huang L, et al. Few-layered SnS_2 on few-layered reduced graphene oxide as Na-ion battery anode with ultralong cycle life and superior rate capability. *Adv Funct Mater*. 2015;25(3):481-489.
15. Lu YY, Zhao Q, Zhang N, Lei KX, Li FJ, Chen J. Facile spraying synthesis and high-performance sodium storage of mesoporous MoS_2/C microspheres. *Adv Funct Mater*. 2016;26(6):911-918.
16. Zhai HF, Xia BY, Park HS. Ti-based electrode materials for electrochemical sodium ion storage and removal. *J Mater Chem A*. 2019;7(39):22163-22188.
17. Cao Y, Zhang Q, Wei Y, et al. A water stable, near-zero-strain O_3-layered titanium-based anode for long cycle sodium-ion battery. *Adv Funct Mater*. 2020;30(7):1907023.
18. Lee J, Koo S, Lee J, Kim D. Rational design of Ti-based oxygen redox layered oxides for advanced sodium-ion batteries. *J Mater Chem A*. 2021;9(19):11762-11770.
19. Lou S., Zhao Y, Wang J, Yin G, Du C, Sun X. Ti-based oxide anode materials for advanced electrochemical energy storage: lithium/sodium ion batteries and hybrid pseudocapacitors. *Small*. 2019;15(52):1904740.
20. Le Z, Liu F, Nie P, et al. Pseudocapacitive sodium storage in mesoporous single-crystal-like TiO_2–graphene nanocomposite enables high-performance sodium-ion capacitors. *ACS Nano*. 2017;11(3):2952-2960.
21. Portenkirchner E, Werner D, Liebl S, Stock D, Auer A, Kunze-Liebhauser J. Self-improving Na ion storage in oxygen deficient, carbon coated self-organized TiO_2 nanotubes. *ACS Appl Energy Mater*. 2018;1(11):6646-6653.
22. Xiong P, Zhang X, Zhang F, et al. Two-dimensional unilamellar cation-deficient metal oxide nanosheet superlattices for high-rate sodium ion energy storage. *ACS Nano*. 2018;12(12):12337-12346.
23. Shi X, Zhang Z, Du K, Lai Y, Fang J, Li J. Anatase TiO_2@ C composites with porous structure as an advanced anode material for Na ion batteries. *J Power Sources*. 2016;330(31):1-6.
24. Liu H, Bi Z, Sun XG, et al. Mesoporous TiO_2-B microspheres with superior rate performance for lithium ion batteries. *Adv Mater*. 2011;23(30):3450-3454.
25. Liu S, Jia H, Han L, et al. Nanosheet-constructed porous TiO_2-B for advanced lithium ion batteries. *Adv Mater*. 2012;24(24):3201-3204.
26. Dawson JA, Robertson J. Improved calculation of Li and Na intercalation properties in anatase, rutile, and TiO_2(B). *J Phys Chem C*. 2016;120(40):22910-22917.
27. Legrain F, Malyi O, Manzhos S. Insertion energetics of lithium, sodium, and magnesium in crystalline and amorphous titanium dioxide: a comparative first-principles study. *J Power Sources*. 2015;278:197-202.
28. Li X, Li W, Li M, et al. Glucose-assisted synthesis of the hierarchical TiO_2 nanowire@ MoS_2 nanosheet nanocomposite

and its synergistic lithium storage performance. *J Mater Chem A*. 2015;3(6):2762-2769.
29. Wu Q, Xu J, Yang X, et al. Ultrathin anatase TiO_2 nanosheets embedded with TiO_2-B nanodomains for lithium-ion storage: capacity enhancement by phase boundaries. *Adv Energy Mater*. 2015;5(7):1401756.
30. Xiang G, Wang YG, Li J, Jing Z, Xun W. Surface-specific interaction by structure-match confined pure high-energy facet of unstable TiO_2(B) polymorph. *Sci Rep*. 2013;3(1):1411.
31. Hu H, Yu L, Gao X, Lin Z, Lou XW. Hierarchical tubular structures constructed from ultrathin TiO_2(B) nanosheets for highly reversible lithium storage. *Energy Environ Sci*. 2015;8(5):1480-1483.
32. Li X, Wu G, Liu X, Li W, Li M. Orderly integration of porous TiO_2(B) nanosheets into bunchy hierarchical structure for high-rate and ultralong-lifespan lithium-ion batteries. *Nano Energy*. 2017;31:1-8.
33. Sun H, Ren YR, Chen ZH, Ding JN. One-step addition of Ag nano-ions to improve the sodium storage capacity of SnS_2/rGO. *Solid State Ion*. 2018;326(15):5-10.
34. Brunauer S, Deming LS, Deming WE, Teller E. Sustainable porous carbons from lignocellulosic wastes obtained from the extraction of tannins. *J Am Chem Soc*. 1940;62(7):1723-1732.
35. Lan K, Xia Y, Wang R, et al. Confined interfacial monomicelle assembly for precisely controlled coating of single-layered titania mesopores. *Matter*. 2019;1(2):527-538.
36. Wu L, Bresser D, Buchholz D, et al. Unfolding the mechanism of sodium insertion in anatase TiO_2 nanoparticles. *Adv Energy Mater*. 2015;5(2):1401142.
37. Chen J, Zhang Y, Zou G, et al. Size-tunable olive-like anatase TiO_2 coated with carbon as superior anode for sodium-ion batteries. *Small*. 2016;12(40):5554-5563.
38. Augustyn V, Come J, Lowe MA, et al. High-rate electrochemical energy storage through Li^+ intercalation pseudocapacitance. *Nat Mater*. 2013;12(6):518-522.
39. Wang J, Polleux J, Lim J, Dunn B. Pseudocapacitive contributions to electrochemical energy storage in TiO_2 (anatase) nanoparticles. *J Phys Chem C*. 2007;111(40):14925-14931.
40. Xu H, Wang W, Qin L, et al. Controllable synthesis of anatase TiO_2 nanosheets grown on amorphous TiO_2/C frameworks for ultrafast peudocapacitive sdium sorage. *ACS Appl Mater Interfaces*. 2020;12(39):43813-43823.
41. Maca RR, Juarez DC, Rodriguez MC, Etacheri V. Nanointerface-driven pseudocapacitance tuning of TiO_2 nanosheet anodes for high-rate, ultralong-life and enhanced capacity sodium-ion batteries. *Chem Eng J*. 2020;391:123598.
42. Wu LM, Bresser D, Buchholz D, Passerini S. Nanocrystalline TiO_2(B) as anode material for sdium-ion batteries. *J Electrochem Soc*. 2015;162(2):A3052-A3058.

SUPPORTING INFORMATION

Additional supporting information may be found in the online version of the article at the publisher's website.

How to cite this article: Liu S, Niu K, Chen S, et al. TiO_2 bunchy hierarchical structure with effective enhancement in sodium storage behaviors. *Carbon Energy*. 2022;1-9. doi:10.1002/cey2.172